A network diagram consisting of various sized light blue circles connected by thin white lines, set against a solid blue background. The circles vary in size and are scattered across the page, with some larger circles acting as hubs for smaller ones.

**Joint Research Programme
BTO 2023.099 | December 2023**

Softsensor flocculatie

Report

Softsensor flocculatie

BTO 2023.099 | December 2023

This research is part of the Joint Research Programme of KWR, the water utilities and Vewin.

Project number

402045/343

Project manager

Martijn van Veggel

Client

BTO - Bedrijfsonderzoek

Authors

Jasper Immink, Martin Korevaar

Quality Assurance

Emile Cornelissen

Sent to

This report is distributed to BTO-participants, it is not a public report.

Keywords

Bedrijfstakonderzoek, Zuivering, Drinkwater, Flocculatie, Modellerling.

Year of publishing
2023

More information

Dr. Jasper N. Immink
T +31 6 25 49 37 99
E jasper.immink@kwrwater.nl

PO Box 1072
3430 BB Nieuwegein
The Netherlands

T +31 (0)30 60 69 511
E info@kwrwater.nl
I www.kwrwater.nl

KWR

November 2022 ©

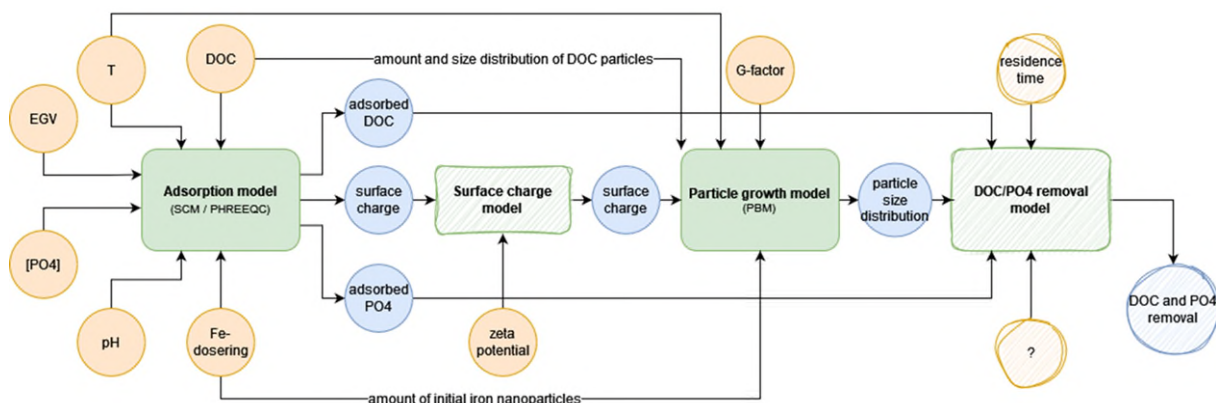
All rights reserved by KWR. No part of this publication may be reproduced, stored in an automatic database, or transmitted in any form or by any means, be it electronic, mechanical, by photocopying, recording, or otherwise, without the prior written permission of KWR.

Managementsamenvatting

Softsensor voor flocculatie: computermodel voorspelt zuiveringscondities op basis van gemakkelijk te meten input en bespaart experimenteerkosten

Auteurs dr. Jasper N. Immink, dr. ir. Martin Korevaar.

Bij de waterzuivering wordt al eeuwenlang coagulatie-flocculatie ingezet: een flocculant (vaak ijzer- of aluminiumchloride) wordt aan water toegevoegd en vormt grote, poreuze clusters, waaraan onzuiverheden adsorberen. Deze clusters zakken naar de bodem en kunnen worden verwijderd. Optimaliseren van dit proces is een tijdrovend en duur proces vanwege de vele variabele procesparameters. Om deze optimalisatie te vergemakkelijken, hebben we voor coagulatie-flocculatie een softsensor ontwikkeld. Dit is een computermodel dat de omstandigheden van het proces kan voorspellen op basis van de toegevoegde flocculantconcentratie en gemakkelijk te meten waterparameters. De softsensor kan in plaats van kostbare en tijdrovende experimenten worden ingezet en helpen om sneller en goedkoper een optimale flocculantdosis te bepalen.



Flowchart van de softsensor zoals nu geïmplementeerd. Oranje cirkels zijn inputparameters, paarse cirkels zijn berekende outputparameters, en groene rechthoeken zijn modelmodules.

Belang: flocculatiecondities voorspellen zonder dure experimenten

Coagulatie-flocculatie is een waterzuiveringsmethode waarin een flocculant (vaak ijzer- of aluminiumchloride) aan water wordt toegevoegd en dan grote, poreuze clusters vormt. Onzuiverheden in het water adsorberen vervolgens aan deze clusters. Onzuiverheden kunnen zo uit de watermatrix worden verwijderd, want de flocculantclusters groeien tot ze zo groot zijn dat ze naar de bodem zakken, waarna ze met onzuiverheden en al

eenvoudig kunnen worden verwijderd. Flocculatie wordt al eeuwenlang ingezet, maar het bepalen van de optimale flocculantdosis bij variabele procesparameters (zoals chemische samenstelling, zoutconcentratie van het influentwater en roersnelheid) blijft een uitdaging voor waterbedrijven omdat al deze parameters de proceseffectiviteit soms beïnvloeden in moeilijk te voorspellen manieren. Experimenten doen en parameters testen is duur vanwege materiaalkosten, manuren en tijdsinvesteringen. Computermodellen

zouden hierbij een grote meerwaarde kunnen hebben, omdat modelvoorspellingen veel goedkoper zijn.

Aanpak: mechanistisch modelleren

Flocculatie is een fysisch-chemisch proces waarin verschillende wetenschappelijke disciplines samenkomen. Door de verschillende onderliggende processen en hun onderlinge interactie in kaart te brengen, kunnen we het gedrag tijdens flocculatie in wiskundige formules vatten. Door die formules in computermodellen te brengen en te voeden met inputparameters als zoutconcentratie en watertemperatuur kunnen de condities in het flocculatieproces worden voorspeld zonder fysieke experimenten.

Resultaat: een werkende en gevalideerde softsensor

De in dit werk ontwikkelde softsensor (computermodel) blijkt in staat het experimentele werk voor onderzoek naar optimale flocculatie-

parameters deels te kunnen vervangen en zo de waterbedrijven kosten te kunnen besparen. De ontwikkelde softsensor voorspelt condities in een coagulatie-flocculatieproces aan de hand van een aantal parameters voor onder andere waterkwaliteit. Alle parameters zijn gemakkelijk te meten.

Implementatie: softsensor inzetten om flocculatiemethoden goedkoper te optimaliseren

Inzetten van de softsensor kan helpen om de zuiveringscondities van een full-scale coagulatie-flocculatieproces te optimaliseren zonder dure experimenten te hoeven doen. Daarnaast kan het gebruik van een softsensor leiden tot een verlaagd gebruik van dure chemicaliën en een betere waterkwaliteit. Verdere investering in de softsensor kan deze helpen tot accuratere voorspellingen te komen voor een breder scala aan watercondities.

Rapport

Dit onderzoek is beschreven in het rapport *Softsensor flocculatie* (BTO-2022.343)

Contents

Report 2

<i>Managementsamenvatting</i>	3
Contents	5
1 General introduction	6
2 Relevant physico-chemical processes	7
3 Model	14
4 Model component validation	20
5 Literature validation	23
6 Typical model results	27
7 Conclusions	30
8 Future recommendations	31
9 References	32
I Brinkman's model	35

1 General introduction

Water treatment companies often deal with ever-changing intake water quality, updates in water quality regulations and changes in material costs used in drinking water. To be able to anticipate these unpredictable changes, engineers would like to predict the effects of such changes: what happens should the chemical composition of inlet water change, can the costs of chemicals be lowered with a more efficient use of these chemicals, or how should processes be designed to achieve a certain level of purification? The answer to these questions can be answered using experimental work, both on laboratory, pilot or full scale, but these are often costly in terms of both time and money. Using a model that predicts certain physical or chemical conditions, within a given uncertainty range, would be able to lighten the need for such costly experiments.

One of the processes which would benefit from a model or softsensor is the coagulation-flocculation process. This process is a widely used treatment process for the production of drinking water or treating waste-water. The process itself has been known for many centuries, with the ancient Egyptians and Romans using versions of the technique. [1] Nowadays, the process is performed by adding a flocculant (often iron or aluminum chloride salts) to water. The flocculant then precipitates, forming large, open structures with a large surface area exposed to the water. Impurities such as dissolved organic carbon (DOC) or phosphate ions adsorb to this surface and are thereby removed from the water. The size of these flocculant clusters allows them to be easily separated from the water: through sedimentation, flotation or filtration. [2]

The ease of operation and the low energy consumption has made coagulation-flocculation ubiquitous, but even though it has been studied for centuries, scientists and engineers still struggle with understanding and predicting its removal efficiencies. [3] In this report, we present and describe a softsensor for this process: a program that interprets the flocculation process, and help to understand and predict removal outcomes. The softsensor takes as input easily accessible measured parameters such as the salt concentration or electrical conductivity of the feed water, iron dosing concentration in the coagulation-flocculation and zeta potential of the created clusters. The softsensor is based on a Population Balance model method, where the size of the clusters is tracked over time by interpreting the different physico-chemical processes that occur during growth and breakdown of these clusters. This size will at a later stage be used to calculate the amount of contaminant molecules that interacts with the coagulant material.

This work builds on previous work by KWR, where specifically the coagulation process itself was studied (BTO 2021.) In this work, a softsensor is built that predicts cluster size and distribution in a coagulation-flocculation treatment technique. The input that this softsensor needs are input parameters that are measurable and readily available to water companies. The softsensor is validated using scientific literature to show that it works as intended, and some output of the softsensor is shown. This softsensor is a great starting point for predicting the conditions and output of a coagulation-flocculation process, and is the necessary foundation for a digital twin of coagulation-flocculation treatment.

2 Relevant physico-chemical processes

In this chapter we discuss the coagulation-precipitation process from a physico-chemical point of view, to give the necessary background for understanding the softsensor implementation.

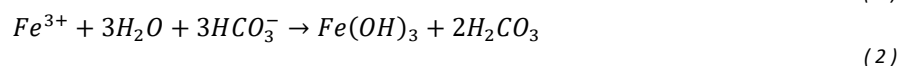
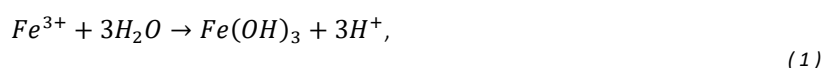
In water treatment technology, coagulation and flocculation are terms that are used to describe a range of phenomena that end with large aggregate clusters to which contaminants adsorb. However, in colloid science and physico-chemical literature, coagulation and flocculation have somewhat different definitions. To avoid any confusion, we will in general use the terms coagulation and flocculation as is understood in water treatment technology. We refer to coagulation when we discuss the process of formation of precipitated material from dissolved material, and we refer to flocculation when already precipitated material encounters other precipitated material, and clusters together through some process.

Overview of precipitation processes

Generally, precipitation and the coagulation-flocculation process occurs through a multi-step process, going through nucleation, growth and aggregation stages. Before any of these stages, the added coagulant material is added and dissolves. [4] This dissolved material immediately hydrolyzes and subsequently is in a metastable state and would energetically favor a solid, often in a crystalline state. In the first stage of the precipitation process (nucleation) the initial crystallites or nuclei form; in the growth stage, dissolved material will deposit molecule by molecule onto a crystallite, growing it larger; and during the aggregation stage, particles encounter other particles, binding to each other, forming clusters until ultimately, the cluster is big and heavy enough to precipitate (or light enough to float out of suspension). Below, we will discuss each of these subprocesses in some detail, taking the example of iron chloride precipitation.

Pre-nucleation: hydrolyzation of iron chloride

Before the process of precipitation occurs, or the zeroth step of a coagulation-flocculation process, the iron chloride is added to the to be treated water. Upon addition, the following chemical reactions take place:



Which specific reaction takes place depends on the pH and the presence of carbonate ions. However, in general all iron is almost instantaneously hydrolyzed to $Fe(OH)_3$. These ferrihydrite-molecules are poorly solvable, with log K-values of -40. [5] With the strong tendency of ferrihydrite to precipitate (out of solution), the iron(III) hydrolysis and subsequent transformation to solid material occurs on a very rapid time scale, on the scale of nanoseconds. [6]

Nucleation and growth

With the formation of (dissolved) ferrihydrite, the nucleation process starts. It comprises of the coagulation of individual and dissolved atoms or molecules into small crystallites, generally starting at 10-100 molecules. [7] It is broadly energetically unfavorable to form such initial nuclei spots, but the subsequent nucleus growth to clusters larger than 10-100 molecules is energetically favorable. The initial nucleus formation is an interplay between water-ferrihydrite interactions and ferrihydrite-ferrihydrite interactions. [8] The latter is much more energetically favorable, and the system will always try to maximize the amount of ferrihydrite-ferrihydrite interaction as compared to water-ferrihydrite interactions. If a ferrihydrite molecule exists in the interior of a crystal, it has maximized its ferrihydrite-ferrihydrite interactions (expressed as bulk free energy in Figure 2), but when it exists at the surface of a crystal, it still has water-ferrihydrite interactions (expressed as surface energy in Figure 2). This is one of the driving forces behind nucleus growth, graphically represented Fig. 1: a crystallite will try to maximize the amount of interior molecules, as they have the most ferrihydrite-ferrihydrite interactions. In the meantime, it will minimize the amount of exterior molecules, as they experience more water-ferrihydrite interactions. This results in nanoparticles that experience a drive to maximize the volume/surface ratio, which can be achieved by growing in size.

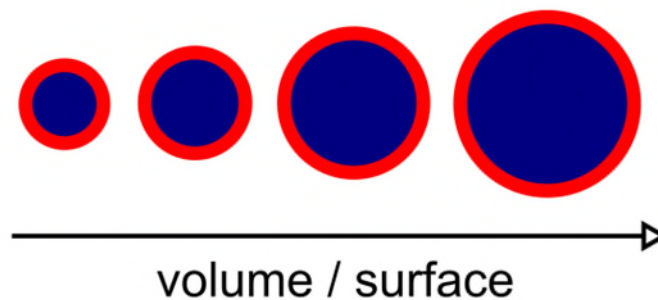


Figure 1: Graphic representation of a growing crystallite, as the crystallite grows its volume-to-surface ratio increases.

These energies together lead to what is graphically represented in Fig. 2: it costs energy to make a crystallite until it overcomes a critical radius; after which growth becomes energetically favorable. There often is a minimum nucleus size, specific for the material and system, due to binding energies being specific to the materials present in the system.

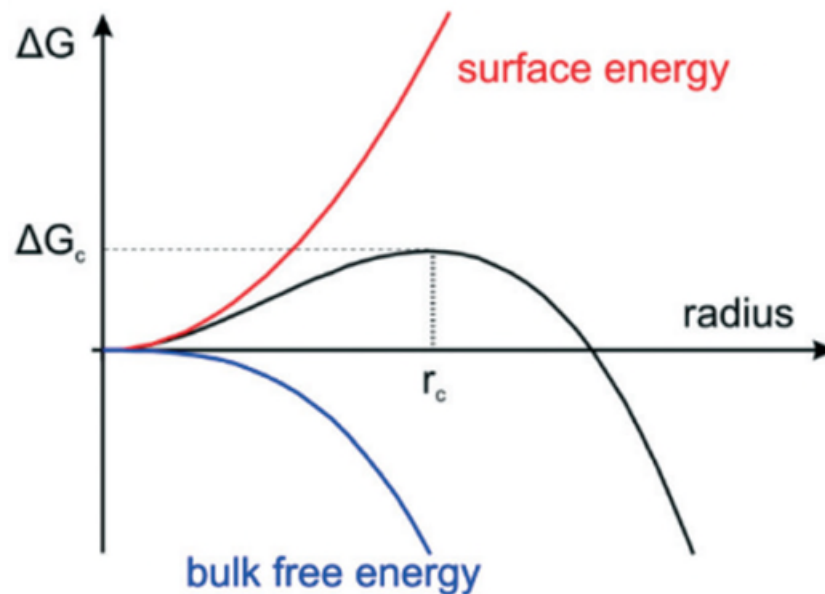


Figure 2: Graphic representation of the interplay between energies in a crystallite. On the y-axis the energy, on the x-axis the radius of the crystallite. As the crystallite grows, the energy gained from the ferrihydrite-ferrihydrite interactions overtakes the energy input from building the ferrihydrite-water surface. From Polte et al.

Because this process possesses an energy barrier, it either needs energy or a catalyst. A typical catalyst is a heterogeneous species in solution onto which crystals can grow, such as a speck of dust, an added seed crystallite or a large, irregular object like a tank wall. In the case that formation of a nucleus does not cost a lot of energy, random thermal fluctuations are enough to form a crystallite. In the case that enough catalytic particles are present in solution, or when crystallite formation does not cost too much energy, nuclei will form homogeneously throughout a sample volume (called a spinodal process). In general, feed waters for drinking water treatment (surface, ground water) contain a sufficient amount of material that can act as seeding material or heterogeneous catalysts, [9] and ferrihydrite is such a poorly solvable molecule that its nucleation is likely spinodal. [10]

If the critical size is reached, dissolved ferrihydrite molecules will deposit onto the now large nucleus, growing it in size. This process continues until there is no more dissolved material left, and until the particle is stable at its current size, or until the particle becomes so big that it sediments/floats (out of solution).

LaMer nucleation/growth mechanism

The ferrihydrite precipitation reaction mechanism as it is applied by water treatment facilities is generally accepted to follow the LaMer mechanism, which slightly deviates from the pathway that has been described in the previous paragraph. In the LaMer mechanism, a chemical is added to a solution, which then reacts and is transformed into a nucleus precursor molecule. The LaMer mechanism is typified by bringing a small volume of a highly concentrated precursor in a larger volume. [8] In our case, ferric chloride is brought into a large volume of water which hydrolyzes into ferrihydrite. The dissolved ferrihydrite concentration is then locally above a certain concentration necessary for spontaneous nucleus formation, known as the critical limiting supersaturation. In these conditions nuclei are formed spontaneously. Quickly after this nucleation process, the dissolved ferrihydrite concentration drops below the critical limiting supersaturation, prohibiting nucleation from being formed. This process leads to nuclei that are very homogeneous in size. Furthermore, in the case of ferrihydrite, the hydrolyzation and nucleation formation is so fast that practically all monomeric ferrihydrite coagulates into nuclei before the system has the opportunity to homogenize in space: the movement speed due to stirring is much slower than the time needed to

form all nuclei. [5] This effectively causes all nuclei to nearly instantaneously form upon entering the feed water, and with a negligible amount of ferrihydrite remaining in solution.

Aggregation

When two particles encounter each other, their interaction depends on their material properties and the system surroundings. In general, they interact in two main ways via: i) van der Waals-attractive forces and (ii) electrostatic-based repulsive forces. The interplay between the two determined whether the two particles will attract or repel. This is graphically depicted in Fig. 3. The van der Waals interaction is constant for a given material and solvent. The electrostatic interaction depends on the charge density on the particles and the salt concentration of the solvent: the higher the surface charge, and the lower the solvent salt concentration, the stronger the repulsion. [11]

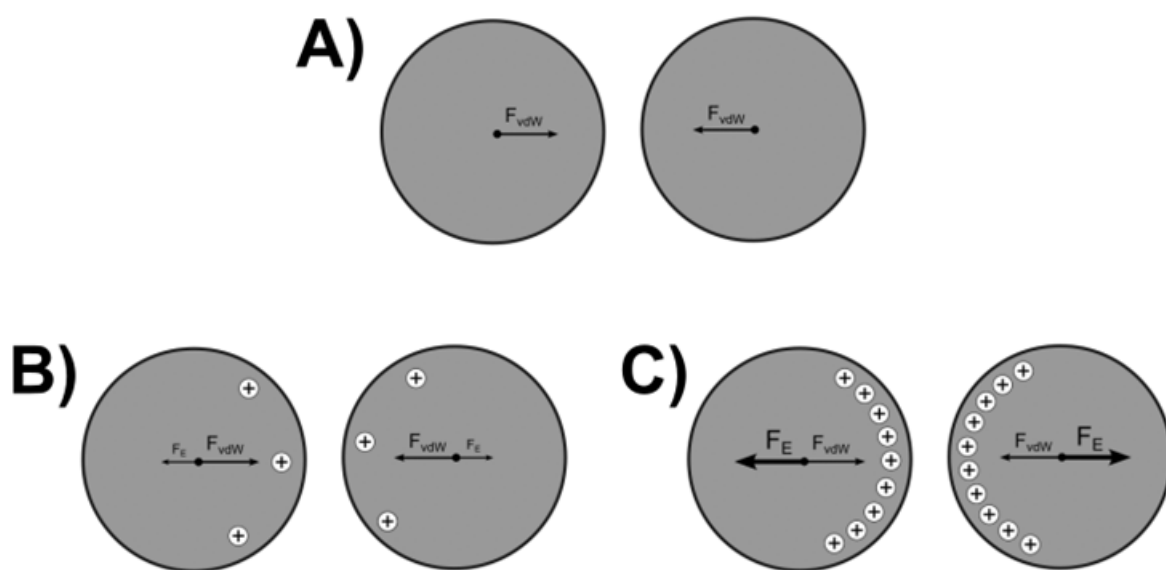


Figure 3: Three different representations of what can happen when two particles encounter. A) The particles have no charge, and no electrostatic repulsion is present. The attractive van der Waals interaction pulls the particles together. B) A small charge is present on the particles, and a weak electrostatic repulsion is present. However, the van der Waals interaction is strong enough to overcome the repulsion. C) A high charge is present, and electrostatic repulsion is strong. The repulsion cannot be overcome by van der Waals attraction.

Calculating the interaction magnitude between two particles is often done by a DLVO-type potential (DLVO stands for the four scientists Derjaguin, Landau, Verwey en Overbeek). Using this DLVO potential, one can calculate an energy barrier that has to be overcome for two particles to aggregate. [12] [13]

Since the van der Waals attraction for a material-medium combination is largely constant, [14] the strength of the attraction between two ferrihydrite-nanoparticles in water is (predominantly) determined by the magnitude of the electrostatic repulsion. This is in turn predominantly determined by the surface charge density on the particles and the salinity of the solvent.

The magnitude of the electrostatic repulsion strongly affects the shape and openness of a final cluster, as graphically represented in Fig. 4. In the case that two particles experience a strong van der Waals attraction, and thus a small electrostatic repulsion, any particle that encounters a cluster will encounter a strong force binding itself to that cluster. It will experience a low mobility after approach, and will likely remain on the position that it initially encountered the cluster. However, if the van der Waals attraction is weaker (and the electrostatic repulsion stronger), then the binding energy between particle and cluster is weaker, and the newly aggregated particle has a

higher degree of mobility. This particle will then be able to move across the surface of that cluster, and find a spot to “nestle” itself into. Clusters with weak electrostatic repulsions will form more open structures, whereas more dense structures are formed with stronger electrostatic repulsions. Finally, should the electrostatic repulsion be too strong, a particle will not be able to approach a cluster, and cluster will not grow at all. [15]

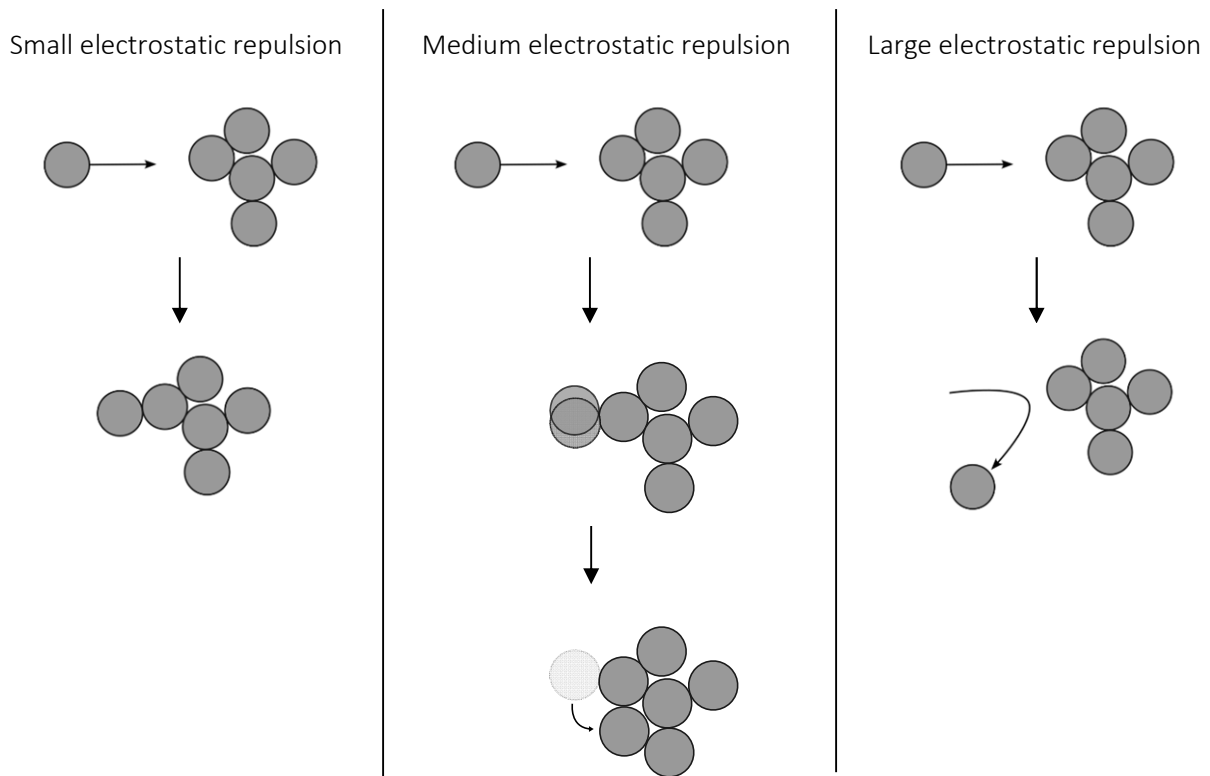


Figure 4: Graphical representation of the aggregative process of a particle encountering a cluster. In the case of small electrostatic repulsions, new particles will remain on the cluster where they found the cluster; with medium electrostatic repulsion, the particle has a degree of mobility after encountering the cluster, allowing rearrangement into a more dense cluster; and with large electrostatic repulsions, no particles will approach the cluster and growth will be inhibited.

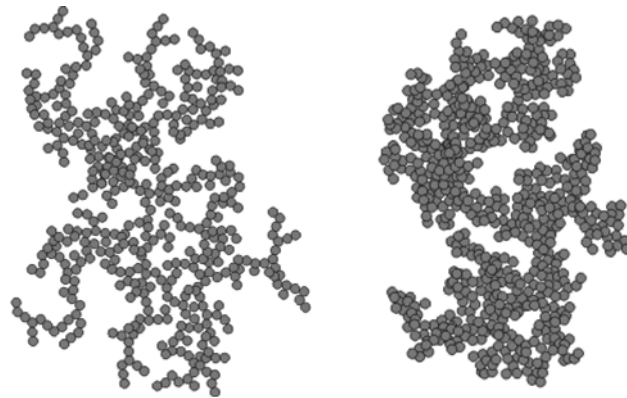


Figure 5: An graphical representation of clusters formed through a more DLCA-dominated mechanism (left) and RCLA-dominated mechanism (right).

The magnitude of the electrostatic repulsion thus governs the structure of the final cluster. Aggregation with weak electrostatic repulsions on particles is also typically described by a Diffusion-limited Cluster Aggregation (DLCA)-process, whereas aggregation with stronger electrostatic repulsions on particles is typically described by a Reaction-limited Cluster Aggregation (RLCA)-process, as seen in Fig. 5. [16] The final shape of the cluster is different for the two types, with DLCA-processes yielding more open clusters and RCLA-processes more compact clusters. [17] This observation is often quantified by a fractal dimension, a measure of the openness of the structure. The fractal dimension has its extremes at 1 (all particles clustered in a one-dimensional line) and 3 (all particles clustered to form a perfectly filled sphere). It can be calculated as follows: [18]

$$N = \left(\frac{d_a}{d_p} \right)^{f_d} \quad (3)$$

with the following parameters:

- | | | |
|---------|-------------------------------------|------------|
| • N | Number of particles in an aggregate | [-] |
| • d_a | Diameter of the aggregate | [m] |
| • d_p | Diameter of the monomeric particle | [m] |
| • f_d | Fractal dimension | [unitless] |

One can define the aggregate diameter in various ways, and often the hydrodynamic diameter is used: [19]

$$\frac{1}{d_H} = \frac{1}{N^2} \left\langle \sum_{i \neq j} \frac{1}{r_{ij}} \right\rangle \quad (4)$$

with the following parameters:

- | | | |
|------------|--|------------|
| • d_H | Hydrodynamic diameter (Aggregate diameter) | [m] |
| • N | Number of particles in an aggregate | [unitless] |
| • r_{ij} | distance between particle i and j | [m] |

The physical meaning of the hydrodynamic radius is that, should the entire cluster be replaced with a solid spherical particle with diameter d_H , the diffusivity of the cluster and replacement particle would be identical. The reason that we use hydrodynamic sizes instead of other definitions is twofold: (i) we will be using a model where we need

to define the diffusive and mobility behavior of individual clusters; (ii) the hydrodynamic radius is not sensitive to very long structures extending outward, and other radius definitions are more sensitive to this behavior. [20] It has been found that, using the above definition, $f_d = 1.7-1.8$ for DCLA and $f_d = 2.0-2.2$ for RCLA. [21] [22] [23] Energetic barriers to aggregation and rearrangements after initial aggregation, such as induced by shear, are related to a rise in f_d . [24]

3 Model

The model that was chosen to represent the coagulation/flocculation process is the Population Balance model. [25] This is a model that is essentially a table, where the current distribution of clusters is recorded and updated as they change over time. Each table column counts the number of clusters in a certain size range. These columns are often referred to as bins, with a bin being like a bucket: each bin is defined by a minimum and maximum size (bin size), and all clusters in the system within that size range are counted in that bucket. The bin value counts how many of these clusters exist in the system.

Then, we define a certain time step (time for which the system is allowed to evolve for one calculation step), and calculate the number of clusters being formed or destroyed during this specific time step. We then update the table using this calculation. Then, using the newly updated table, we determine a new time step, update the table, and so forth.

Since we expect the largest clusters to comprise upwards of 10^{12} nuclei-sized particles, we cannot have one bin per individual cluster size. [26] Therefore, we use a model with logarithmically increasing binning: the range of the number of particles (or cluster size, as the cluster size increases monotonically with number of particles) increases logarithmically with increasing bin, that is: clusters in bin $i+1$ consist of twice as many particles as clusters in bin i .

It has been shown that ferrihydrite nuclei formed through the LaMer mechanism are around 2-8 nm in diameter. [27] [28] We initialize our system by assuming that all iron added to the system reacts to form ferrihydrite nuclei of this size, which homogeneously distributes through the sample volume. We can make this assumption as we know the formation mechanism is a LaMer mechanism, and as we described above, formation occurs on a very short time scale, much shorter than stirring time scales. [6] [29]

We can calculate the number of nuclei added to the system by considering that:

$$V_{Fe(OH)_3} = N_p \cdot \frac{4}{3} \pi r^3 \quad (5)$$

$$V_{Fe(OH)_3} = \frac{m_{Fe(OH)_3}}{\rho_{Fe(OH)_3}} \quad (6)$$

$$m_{Fe(OH)_3} = m_{Fe}(\text{added}) \cdot \frac{M_{Fe(OH)_3}}{M_{Fe}} \quad (7)$$

with the following parameters:

- $V_{Fe(OH)_3}$ Volume of ferrihydrite added [m³]
- N_p Number of ferrihydrite particles formed [-]
- r Radius of ferrihydrite particles formed [m]
- $m_{Fe(OH)_3}$ Mass of ferrihydrite formed [kg]
- $\rho_{Fe(OH)_3}$ Density of ferrihydrite [kg m⁻³]
- $m_{Fe}(\text{added})$ Added mass of iron (via iron chloride) [kg]
- $M_{Fe(OH)_3}$ Molar mass of ferrihydrite [kg mol⁻¹]
- M_{Fe} Molar mass of iron [kg mol⁻¹]

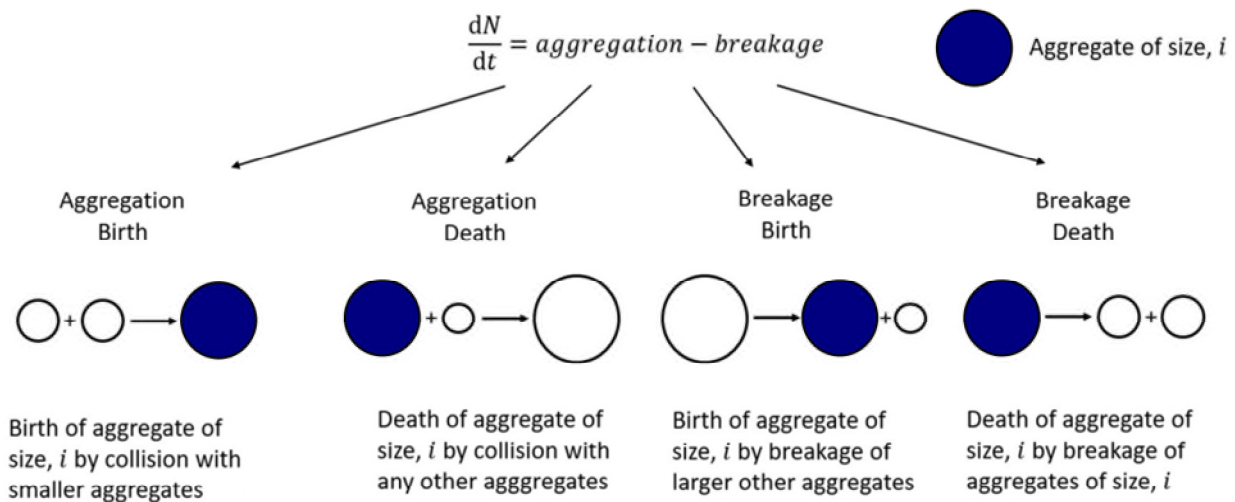


Figure 6: Explanation of the Population Balance Model, adapted from [10].

Equation 8 is also graphically represented in Fig. 6. The first two terms of the equation (the first row of equation 8) govern the “birth” of clusters of size i due to aggregation of two species smaller than i ; the third and fourth term (second row) govern the “death” of a cluster of size i due to it aggregating with any another cluster, the result of which will end up in a bin larger than i ; the fifth term governs the birth of a cluster of size i due to a larger cluster breaking up into one or more clusters of size i , and the sixth term governs the death of an aggregate due to it breaking up.

There are several assumptions that are made in a population balance model. The first is that all clusters have the same “shape”, that is, all clusters of size i have the same fractal dimension. This is a reasonably safe assumption, as all clusters evolve via the same path and in the same conditions. It also assumes that the system which is described (in this case, the flocculation growth basin) is homogeneous and all clusters are homogeneously distributed throughout the system. This is a relatively safe assumption, but breaks down at very large cluster sizes, as particles will sediment. There are several methods to compensate for this, but since this is not expected to have a large effect, these effects will be addressed in future iterations of this model. It’s also assumed that no *fractionation* occurs: with fractionation we mean that a single clusters breaks up into three or more clusters in a single timestep. This means that we assume that all fractioning processes occur via a break-up into two clusters and subsequently break up into two further clusters. This assumption has been shown to be safe and valid as long as the timestep duration is small enough. [26]

The basic building block of a floc is the ferrihydrite particle of 2-8 nm, and to be able to calculate the model using the population balance equation, we need to determine four parameters: the collision efficiency α , the collision frequency $\beta_{i,j}$, the breakage distribution $\Gamma_{i,j}$ and the breakage frequency S_i . We will discuss these four terms here below.

$\alpha_{i,j}$ – collision efficiency

We use DLVO theory to determine an energy barrier for aggregation: if two particles collide, this energy barrier has to be surmounted if a collision also leads to aggregation. From the energy barrier, we can use the Arrhenius equation to calculate a probability of a successful collision. [30] DLVO theory comprises the addition of (i) screened electrostatic potential and (ii) van der Waals attraction:

$$\alpha_{i,j} = e^{\frac{-E_a}{kT}}$$

(9)

$$\frac{U_{Yuk}(d_{ctc})}{kT} = Q^2 \lambda_B \left(\frac{e^{\kappa\sigma}}{1 + \kappa\sigma} \right) \frac{e^{-\kappa d_{ctc}}}{d_{ctc}}$$

(10)

$$\frac{U_{vdW}}{kT} = -\frac{A}{6} \left(\frac{2r_i r_j}{d_{ctc}^2 + (r_i + r_j)^2} + \frac{2r_i r_j}{d_{ctc}^2 - (r_i - r_j)^2} + \ln \left(\frac{d_{ctc}^2 - (r_i + r_j)^2}{d_{ctc}^2 - (r_i - r_j)^2} \right) \right)$$

(11)

$$\kappa^{-1} = \left(\frac{\epsilon_r \epsilon_0 kT}{e^2 \sum_i c_i z_i^2} \right)^{\frac{1}{2}}$$

(12)

$$d_{ctc} = r_i + r_j + r$$

(13)

with the following parameters:

• $\alpha_{i,j}$	Collision efficiency	[-]
• E_a	Energetic barrier for aggregation	[kg m ² s ⁻²]
• k	Boltzmann constant	[kg m ² s ⁻² K ⁻¹]
• U_{Yuk}	Yukawa or screened electrostatic potential	[kg m ² s ⁻²]
• Q	Effective colloidal charge	[A s]
• λ_B	Bjerrum length	[m]
• κ	Inverse Debye length	[m ⁻¹]
• σ	Diameter of the charged particles	[m]
• U_{vdW}	van der Waals potential	[kg m ² s ⁻²]
• d_{ctc}	Center-to-center distance between two particles	[m]
• A	Hamaker constant, defined for material/solvent	[kg m ² s ⁻²]
• ϵ_r	Dielectric constant of the solvent	[-]
• ϵ_0	Permittivity of free space	[kg ⁻¹ m ⁻³ s ⁴ A ²]
• e	Elementary charge	[A s]
• c_i	Concentration of ion i	[m ⁻³]
• z_i	Valency of ion i	[-]

All of these parameters are known physical constants or are input parameters, with only a few input parameters varying. This then becomes an exercise in filling in the parameters correctly: k , T , λ_B , σ , ϵ_r , ϵ_0 , e , c_i , z_i and A are all natural constants or specific parameters for ferrihydrite in water with a known salinity. We determine the potentials U_{Yuk} and U_{vdW} as a function of d_{ctc} , and from the combination of the two we determine E_a . This is graphically represented in Fig. 7. From E_a we can determine $\alpha_{i,j}$ using the above Arrhenius equation.

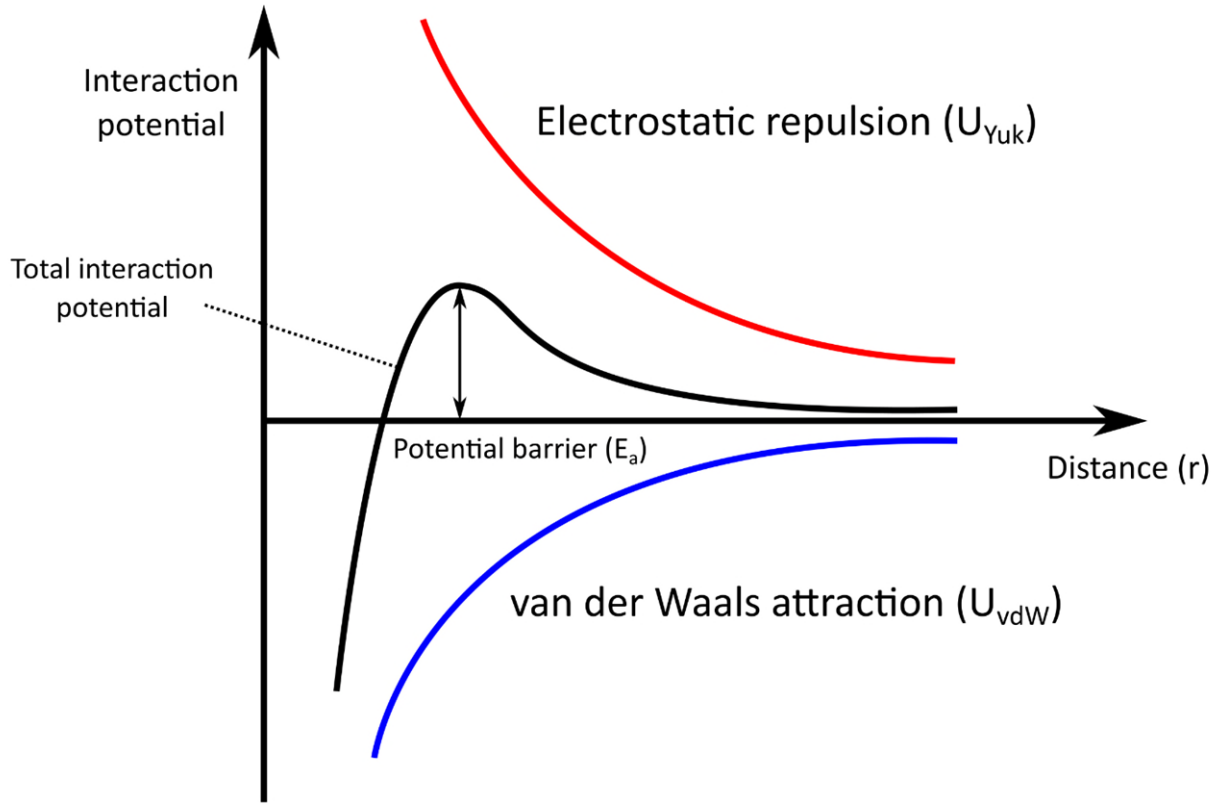


Figure 7: Typical DLVO potential. On the x-axis the distance between two particles, and on the y-axis the interaction potential or energy. The red line is the electrostatic repulsion and the blue line is the van der Waals attraction; the combined DLVO potential is black. If summed, it leads to an energy barrier that can be calculated. Schematic from Guven et al. [31]

It should be noted that E_a is directly defined by U_{Yuk} and U_{vdW} , with the energy barrier being extracted from the sum of the two. It is defined as the maximum of the DLVO potential (formally minus the long-distance DLVO-potential, but this decays to zero for distances that are common in our system). [32] [11] [33] [34] [35] [36] Also, we note that the Arrhenius equation calculates the probability of an event with energy barrier E_a occurring, with kT being the energy that the system provides. kT is the energy of a random thermal fluctuation, i.e. the amount of energy provided if only thermal energy is present in the system. In our case, kinetic energies play a significant role and can cause collisions to overcome the energy barrier. It could therefore an expansion of the model to, instead of kT , use a term that is dependent on the kinetic energies present in a collision. [37]

$\beta_{i,j}$ - collision frequency

There are three processes that can lead to the interaction of two particles : (i) collisions due to diffusion; (ii) shear-induced collisions; and (iii) two clusters sedimenting at different rates. [26] All of these processes are relevant to the process, as they happen at different moments in the coagulation-flocculation process. For each of these processes, we can define a collision rate based on the specific process, and add the three to get to the combined collision frequency. These formulas are based on literature . [38]

$$\beta_{i,j} = \beta_{Br} + \beta_{Sh} + \beta_{DS} \tag{14}$$

$$\beta_{Br} = \frac{2kT}{3\mu} \left(\frac{1}{\Omega_i R_i} + \frac{1}{\Omega_j R_j} \right) (R_i + R_j) \tag{15}$$

$$\beta_{Sh} = \frac{1}{6} G (\sqrt{\eta_i} R_i + \sqrt{\eta_j} R_j)^3 \quad (16)$$

$$\beta_{DS} = \pi (\sqrt{\eta_i} R_i + \sqrt{\eta_j} R_j)^2 |u_i - u_j| \quad (17)$$

• $\beta_{i,j}$	Total collision frequency	$[s^{-1} m^{-3}]$
• β_{Br}	Collision frequency due to diffusion	$[s^{-1} m^{-3}]$
• β_{Sh}	Collision frequency due to shear	$[s^{-1} m^{-3}]$
• β_{DS}	Collision frequency due to sedimentation	$[s^{-1} m^{-3}]$
• μ	Dynamic viscosity of the fluid	$[kg m^{-1} s^{-1}]$
• Ω_i	Drag force correction	[-]
• R_i	Radius of particle i	[m]
• G	Shear rate	$[s^{-1}]$
• η_i	Fluid accumulation efficiency	[-]
• u_i	Settling velocity of a permeable cluster	$[m s^{-1}]$

These equations can be fully solved, if the shear rate and the temperature of the system are known. The drag force correction, fluid accumulation efficiency and settling velocities are calculated using a mathematical method known as Brinkman's extension of Darcy's law, described in Appendix I. [38] [39] The only parameters that are necessary for calculating Ω_i and η_i are monomeric particle radius, cluster radius and fractal dimension, all known or defined parameters as described in equations 5-7. Because of the verbosity of Brinkman's model, it can be found in the appendix.

$\Gamma_{i,j}$ – Breakage distribution kernel

The breakage distribution kernel defines how large the fragments resulting from a break-up event are, i.e. what bin they will fall in. There are many different options, and we have implemented that when a break-event occurs, the two resulting fragments end up in the bin directly below the bin of the source cluster, breaking up into two roughly equally-sized clusters. It is known that this simple kernel can capture real-life cluster dynamics well. [26]

S_i - Breakage distribution rate

Breakage models are exclusively empirical models, fitted to existing data since no mathematical models exist to predict this through first principles. [40] The reason for this is that it is a highly complex process where a large number of small effects can have a large influence on the final breakage event. We therefore implement an empirical power law model, used often in modeling ferric hydroxide cluster growth in stirred chambers:

$$S_i = P_1 G^{P_2} R_i^{P_3} \quad (18)$$

• S_i	Breakage rate	$[m^3 s^{-1}]$
• G	Shear rate (G-factor)	$[s^{-1}]$
• R_i	Hydrodynamic radius of cluster	[m]
• P_1	Fit parameter 1	[-]
• P_2	Fit parameter 2	[-]
• P_3	Fit parameter 3	[-]

Here, we fill in the three fit parameters to be $9.0 \cdot 10^{-7}$, 0.71 and 0.33, respectively, according to the work by Pandya et al., [41] which investigated iron hydroxide clusters in stirred suspensions.

4 Model component validation

In this chapter we discuss the different validation steps to show that the model are working as intended. In the next chapter we focus on the model as a whole. Here we will show the three biggest equation steps: (i) the DLVO equation, (ii) the collision frequency and (iii) the Population Balance Equation integrated.

DLVO Equation

We used our implementation of DLVO theory to validate the full interaction potential at different salt concentrations, using the parameters from the work of Liu et al. [32] This is work on polystyrene colloids, which only requires tuning of the Hamaker constant to make the softsensor apply to this other material.

This results in the full DLVO plots indicated in Fig. 8. The figures A and B in figure 8 do correspond which shows us that our implementation of DLVO was correct.

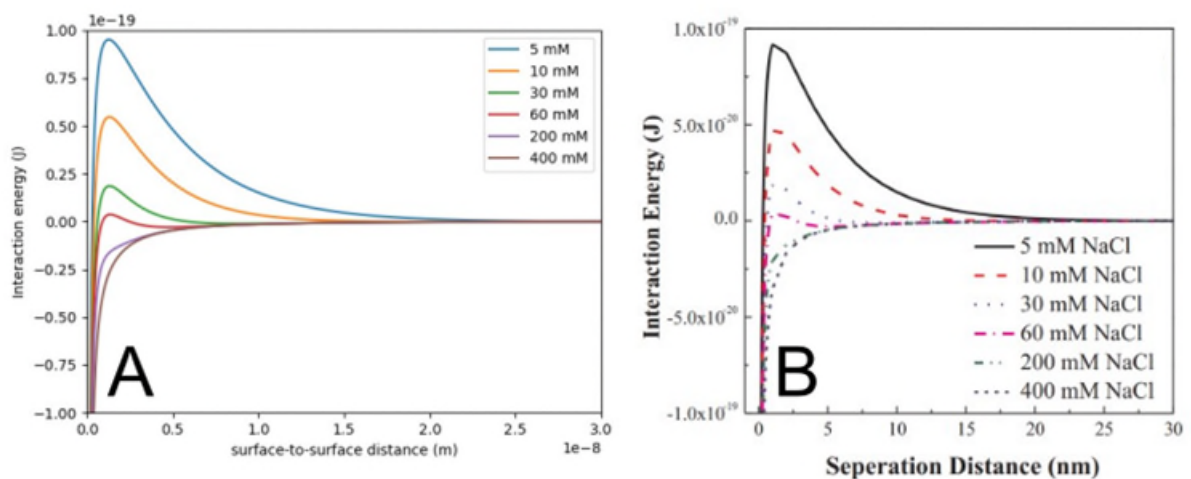


Figure 8: Plots of the full DLVO equation from A) our calculations, B) calculations from [15]. Our calculations took the parameters from their papers to mimic their results.

Collision Frequency

The validation of the collision frequency was performed in two steps. First, we directly compared a simplified version of our model with scientific literature (not the model described in the previous chapter); thereafter, we check the differences between our simplified and our full model as described above with the scientific literature. Our simplified model is a model where we do not account for porosity, and correction terms such as the fluid collection efficiency and drag force correction. It can be found in [26], and results in the image as seen in Fig. 9. The figures A and B (Figure 9) are very similar which indicates a successful validation of this implementation.

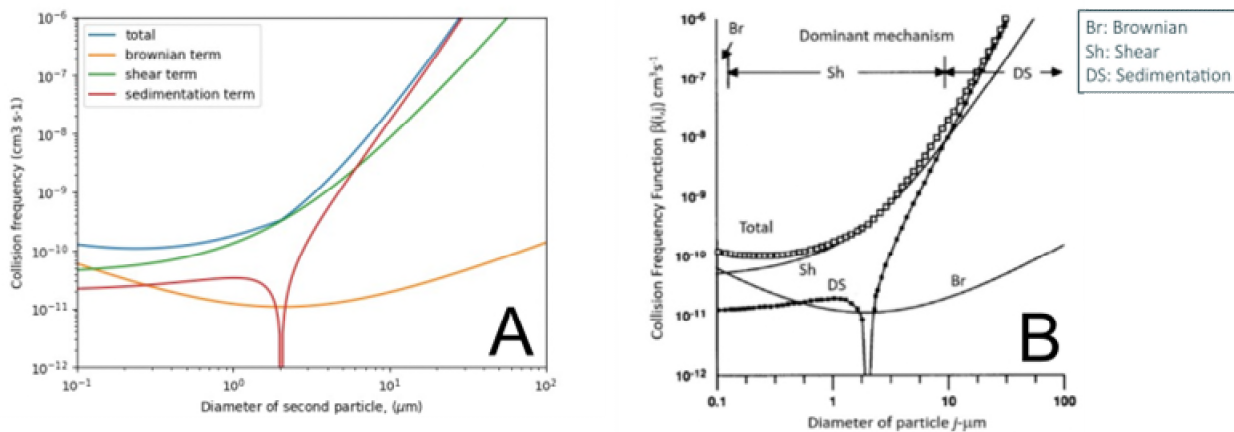


Figure 9: Plots for the simplified collision frequency model calculations. A) our calculations, B) calculations from [26]. In these plots, the collision rate of a cluster of a given size with another cluster of diameter $2 \mu\text{m}$ is plotted at $G=18 \text{ s}^{-1}$. Three different subfrequencies are plotted, corresponding to the different subterms in the collision frequency.

The simplified collision model assumes clusters to move as if they are completely solid inside the hydrodynamic radius, which is not the case with fractal-like clusters as a representation of ferrihydrite clusters. We corrected our model with the suggestions of [26], however: it should be noted, however, that no published articles exist where the implementation was done as we have described it, so we have to rely on qualitative checking and manual checking of the implemented values. We find that our implemented model corrects for collisions between large fractal aggregates, which is in line with the prediction from the paper. [26] We have calculated the differences between the models by hand and find that our implementation predicts the same results. Examples of plots where the differences are calculated can be found in Fig. 10, where the collisions of a cluster with a given size with a monomeric cluster is plotted. It should be noted that if particles form through a LaMer mechanism, the amount of dissolved monomer can be neglected.

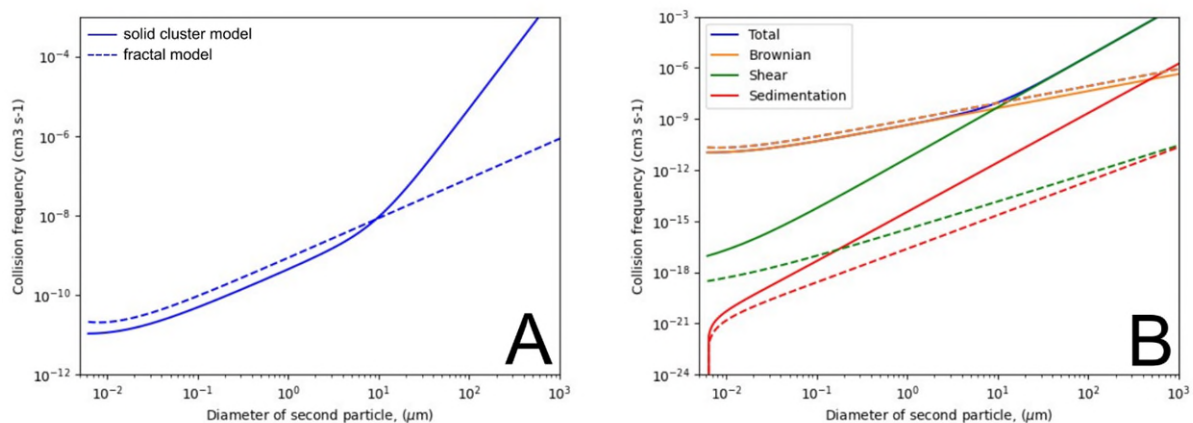


Figure 10: Plots for the fractal collision frequency model calculations as compared to the solid cluster model. A) The model with all subterms added together. B) Two models with all subterms separately plotted. The collision rate of a cluster of a given size with a monomeric precursor is plotted. It can clearly be seen that the larger the second particle is, the larger the discrepancies between the two models is, which corresponds to what is described by Jeldres et al.

Population Balance Equation

Due to the complexity of the population balance equation, we validate it by implementing the six subterms separately and presenting their results with a range of testing initial states and parameters $\alpha_{i,j}$, $\beta_{i,j}$, $\Gamma_{i,j}$, S_i . At the same time, we implement the same equations in Excel with the same dummy parameters. We then directly compare the output of both Excel and our program for each subterm and for the total term, for the first ten iterations. As soon as all subterms and the total term correspond to at least ten decimal points, we can safely conclude that the Population Balance Equation is correctly implemented.

5 Literature validation

In this chapter, we compare the results from the complete model with literature results. We validate our models using experimental results from Ahmad *et al.* [42] Here, iron chloride is added to a tank containing 5L of water under continuous stirring. The salt concentration in the tank and all other parameters necessary for our model, except the fractal dimension, are given in Table 1. In the following, we aim to reproduce their Figure 2a.

First, it is noted that the article deviates from the model in two distinct ways. First, the iron chloride addition to the reactor vat is different in the article and our model: the article describes iron chloride addition through addition of the solid, whereas a population balance model assumes homogeneous concentration throughout the sample. [26] This would mean that our model would underestimate the real cluster sizes, as higher (local) concentrations lead to much faster growth. It should also be noted that iron addition is very low as compared to commercial use. Secondly, the experimental sampling methods are different: the article describes that “collection of suspension samples [...] which were filtered over 0.45 μm filters. [...] The samples were prepared for subsequent analysis.”. We interpret this as samples filtered first, after which the particle size distribution was not immediately measured, and particles will continue to grow in the interim. As this exact sampling sequence is not modeled, our model will again underestimate the results. Therefore, we expect that our model predicts lower values than what is observed in the experiments. While we can alleviate for the first reason for discrepancy (which we will discuss later in this chapter), the second reason cannot be compensated for without additional information. Due to a lack of time and low availability of alternatives, we chose to validate our model using these results.

Table 1: input parameters validation model

Parameter	Value
Added iron [mg L^{-1}]	$2.8 \cdot 10^{-4}$
Particle concentration [m^{-3}]	$1.0 \cdot 10^{17}$
Particle diameter [m]	$1.6 \cdot 10^{-8}$
Salt concentration [mol m^{-3}]	$6.6 \cdot 10^0$
Zeta potential [V]	$-2.6 \cdot 10^{-3}$
Shear rate [s^{-1}]	$1.8 \cdot 10^1$
Time [s]	$3.6 \cdot 10^3$
Temperature [K]	$2.93 \cdot 10^2$

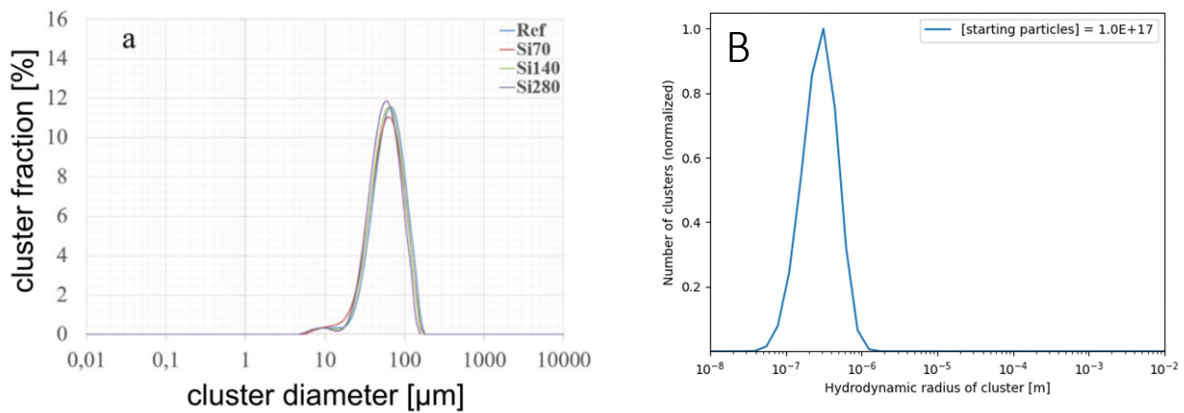


Figure 11: Figure 2a from Ahmad et al., and model output given similar parameters. The model prediction is off by more than two orders of magnitude. Note that the resolution of the model plots is rather low, the reason for this is the logarithmic scale of the bins in the model. This is explained in the second paragraph of Chapter 3.

The first test using the parameters as shown in Table 1 gives the results as shown in Figure 11. With using a generic fractal dimension of 2.0, we observed that the cluster size results from experiment is significantly higher than the cluster size that the model predicts. We therefore test to see what effect the fractal dimension and iron concentration have on the distribution of the clusters.

Fractal dimension

We tested different fractal dimensions settings to mimic the cluster size distribution as reported in literature. For the extremes, we take a reasonable range ranging from 1.7 (diffusion-limited cluster aggregation) to 2.1 (reaction-limited cluster aggregation). [43] While clusters made with pure ferrihydrite are reported, [44] and expected, [17] to have fractal dimensions close to 1.7 due to the character of the aggregation, DOC and other negatively charged material can increase this value far beyond 2.1. [45] [46] [47] Since the current model is based on only ferrihydrite aggregation, we do not go beyond 2.1 for the fractal dimension, with the most relevant value being 1.7, as theory and experimental literature predict this value.

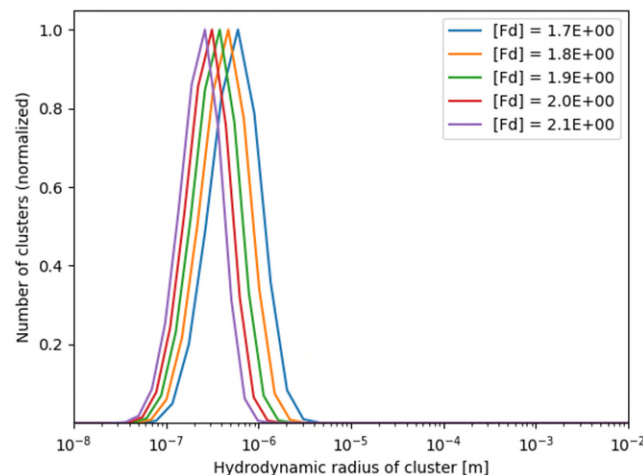


Figure 12: Model output for different fractal dimensions.

In Fig. 12, these different fractal dimensions are plotted, and it is observed that while more open structures do lead to increasingly large clusters, this does not have the effect of fully alleviating the discrepancy between the experimental observations and model predictions.

Particle concentration

The effects of initial particle concentration have a strong effect on the final cluster distribution (Figure 13) more than enough to bridge the discrepancies between model output and experiment. This would imply that to obtain realistic floc sizes, we would need much higher concentrations. A good note to place here is that realistic systems often use such high concentrations, but we are trying to mimic the depicted experiment here.

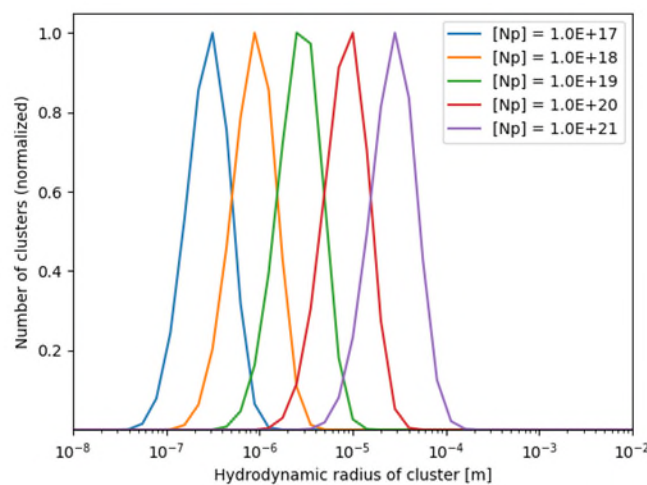


Figure 13: Results with a varying starting particle concentration.

However, the standard version of the model disregards the fact that in reality, ferrihydrite precursor is added to the sample tank by adding concentrated iron chloride. This means that initially, on a local scale, the concentration of particles is much higher. In this locally higher concentration, the cluster size distribution will be pushed to larger sizes, which is expected to have an impact on the final particle size distribution. Since the particle concentration significantly affects the final particle distribution of particles, we implemented a method to check how an initially higher concentration affects the final cluster size distribution.

We do this by modelling the concentration development as follows. Initially, all particles exist in the smallest possible volume: the volume in which all particles reside initially is equal to the total particle volume. This is calculated by calculating the total volume of particles V_p in the system, and then recalculating the final particle concentration assuming that they all reside in that V_p . We then assume that the initial concentration decreases over time with:

$$C_t = C_0 \cdot e^{-3t}$$

- C_t Particle concentration at time t [m-3]
- C_0 Initial particle concentration [m-3]
- t Time [s],

and the factor 3 being necessary for the fact that concentration is a volume-dependent variable which scales with the distance cubed. We then decrease the concentration stepwise, multiplying the concentration with a factor e^{-3} every timestep τ . This timestep is calculated using the formula:

$$\tau_i = \tau_0 \cdot e^i,$$

- τ_i Timestep size of interval i [s]
- τ_0 Initial timestep size [s]
- i Interval number [],

where i is the interval number of the step taken. We can tune the steps taken by tuning τ_0 . We can then define a *dilution time*, which is the time that is necessary for the system to fully change to the final state which is the particle concentration as depicted in Table 1. Before the dilution time, the concentration follows an exponential function with negative exponent, after dilution time the concentration is constant. Using our model with this method, we obtain results as depicted in Figure 14.

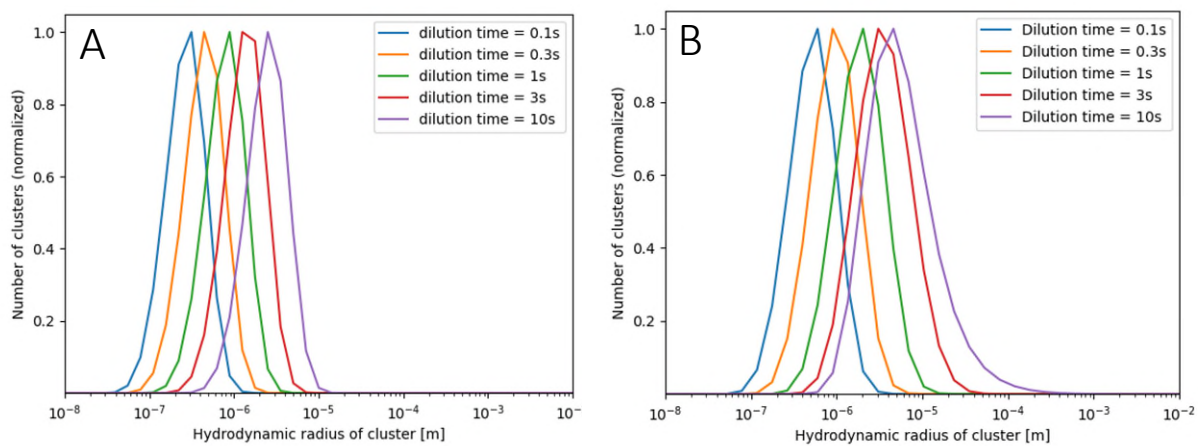


Figure 14: Results with progressive dilution series. A) Fractal dimension is 2.0, B) Fractal dimension is 1.7.

It is immediately obvious that higher starting concentrations which dilute over time have strong effects on the final cluster size distribution. We see from Figure 14 that a slow homogenization process over the course of 10 seconds leads to a population distribution with its peak more than an order of magnitude higher. This is a relatively slow but not unreasonable timeframe.

Tuning the fractal dimension and particle concentration within reasonable limits allows us to clearly approach the results as obtained during the experiments in [40]. Note that there exists a time difference between formation and measurement, which causes particle sizes to be overestimated. The results seen in Figure 14B at the highest dilution times are off by approximately a factor of 3 as compared to the results obtained by Ahmad *et al.* In the validation experiment, the tank size was 5L and stirring was done with a stirrer at 100 rpm, which means that homogenation time should be at least several seconds. Furthermore, we should keep in mind that we model the flocs at fractal dimensions of 2.0, and far smaller fractal dimensions of for example 1.7 are expected for DLCA-clusters. [44] [17]

We have approached the validation experiment as close as possible here, but several discrepancies still exist. Additionally, several parameters such as the influence of pH are not tested. Since no other work exists as far as we are aware, we believe that the next validation step should be to validate our model with our own experimental work, rather than further fine-tune input parameters. However, experimental work is beyond the scope of this specific project, and we intend to perform experiments in future projects.

6 Typical model results

In this chapter we discuss some typical output from our model while varying several parameters, notably fractal dimension, shear rate and salt concentration, that reflect industry operation. Standard parameters can be found in Table 2.

Table 2: input parameters results

Parameter	Value
Added iron [mg L ⁻¹]	10
Particle concentration [m ⁻³]	3.6 · 10 ²¹
Particle diameter [m]	1.6 · 10 ⁻⁸
Salt concentration [mol m ⁻³]	1.0 · 10 ⁰
Zeta potential [V]	2.0 · 10 ⁻²
Shear rate [s ⁻¹]	2.0 · 10 ³
Time [s]	1.0 · 10 ⁴
Temperature [K]	2.93 · 10 ²
Fractal dimension []	2.2

These parameters are chosen to mimic initial stages in a coagulation-flocculation reactor. Using these parameters, we obtain a time series as depicted in Fig. 15. Note that here we depict our results in absolute numbers (SI-units, m⁻³) instead of normalized numbers. Please note also that these are results with instantaneous homogenization.

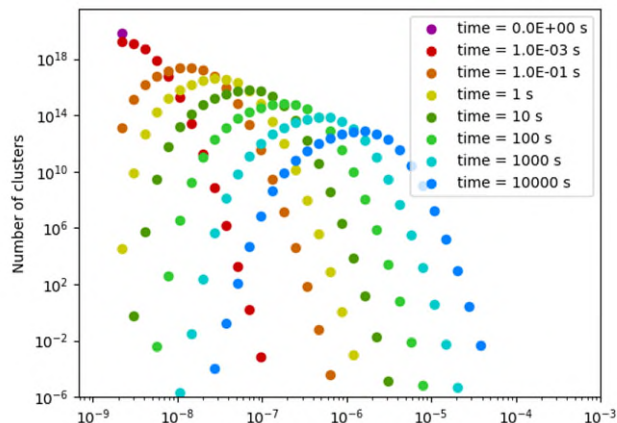


Figure 15: Time series using parameters reflecting industry operation.

A first observation is that cluster size evolves towards the micrometer scale in the time span of one to several hours. We also observe that the evolution occurs on a logarithmic time scale: initial evolution occurs fast and slows down progressively. This is consistent to the timescales of coagulation-flocculation-processes during experimental observations in which the evolution of particle size distributions tends to plateau off over time. [48]

In Figs. 16 we show that tuning the fractal dimension shows us that it can significantly affect the distribution of particles. We tune the fractal dimension between 1.9 and 2.6, values that correspond with experimental observation of clusters in the presence of DOC. Fig 16A shows the final distribution after 10^5 seconds, and we see that we can tune the distribution over two decades of hydrodynamic diameters using this parameter. While smaller fractal dimensions immediately mean larger hydrodynamic diameters, it also leads to higher aggregation rates and thus a larger growth. Fig. 16B shows the mean radius of all the clusters, where the same observations can be observed.

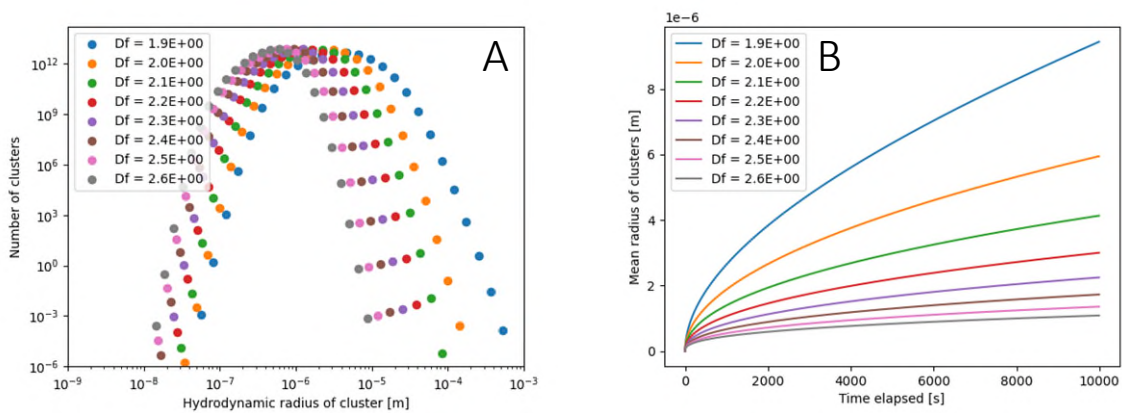


Figure 16: Effects from varying fractal dimension on the cluster distribution after 1 hour. A) final cluster distribution. B) average cluster size over time.

In Figs. 17 we show the effects from tuning the shear rates. Fig 17A shows the final distribution after 10^5 seconds, and we can see that increasing shear rates leads a widening of the cluster size distribution : the distribution will form both larger and smaller clusters. This is due to two counteracting phenomena acting on the distribution. While the high shear rates lead to the more frequent break-up of clusters, the higher shear rates also bring clusters more often together, increasing the aggregation rates. Nonetheless, it should be said that this effect was only observed for unrealistically high shear rates. One can interpret this by assuming that in real systems, this type of behavior could only occur in localized regions of high shear, such as turbulent regions. This is, however, in our

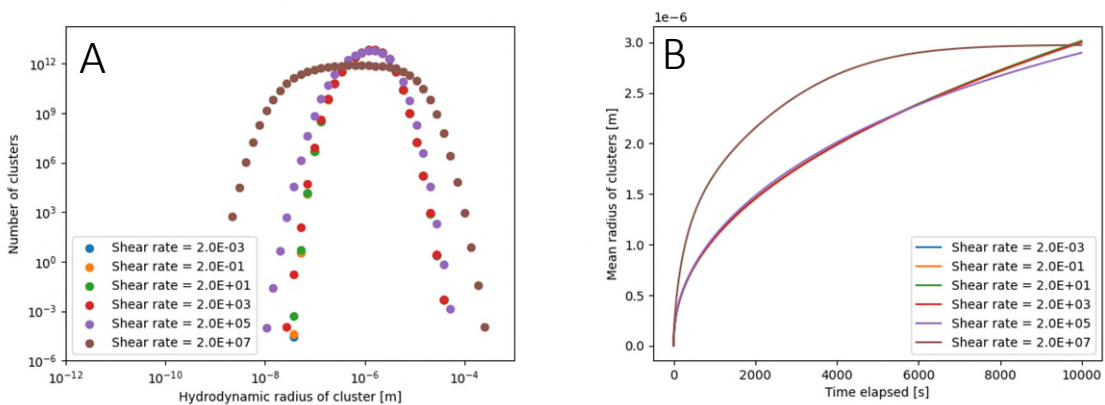


Figure 17: Effects from varying shear rates on cluster distribution after 1 hour. A) final cluster distribution. B) average cluster size over time.

opinion, not representative behavior as the shear rates are unrealistically high, and the future incorporation of DOC into the model will change the shear-dependent behavior. However, since the size and charge differences between ferrihydrite and DOC can lead the rheological behavior of clusters (and the system as a whole) to be unpredictable, it is difficult to make any quantitative prediction on how the DOC incorporation will change the behavior.

In Figs. 18 we see that tuning the ionic strength shows a rather small effect on the cluster size distribution. We tune the salt concentration between concentrations roughly corresponding to drinking and sea water salinities, and we see that neither extreme affects distribution much. This is both an interesting observation and a reflection of reality: the salt concentration primarily affects the aggregation probability; that is, the probability that two clusters stick after encounter. We currently model pure ferrihydrite, which in our conditions tends to aggregate readily [11] indicating that electrostatic repulsion is in this case not much of an issue. Electrostatic screening effects then do not affect much, and salinity does not have a strong effect. Note that upon incorporation of DOC in the model, this changes: ferrihydrite in the presence of DOC like humic acid can become strongly negatively charged due to humic acid-adsorption, and the Coulombic interaction between such clusters can become dominant again. In this case, salt becomes an important factor.

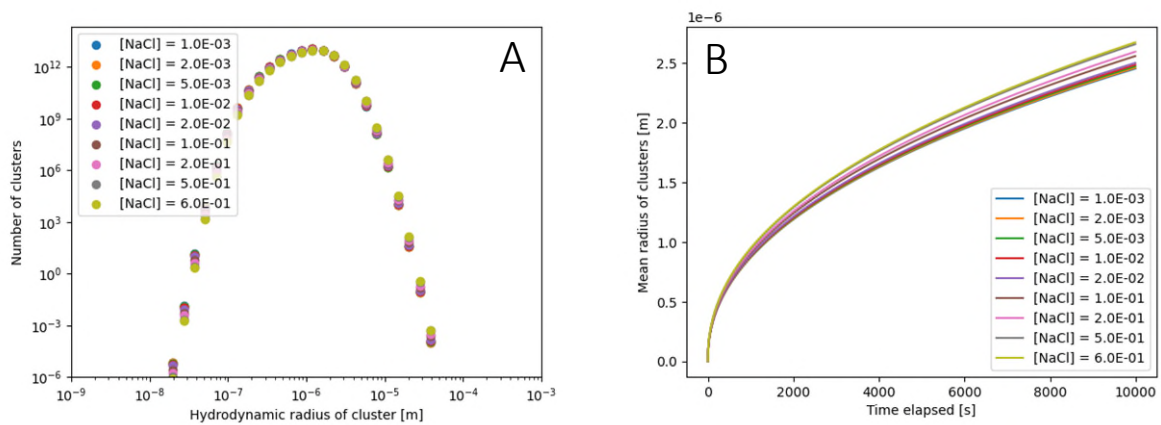


Figure 18: Effects from varying salt concentration on cluster distribution after 1 hour. A) final cluster distribution. B) average cluster size over time.

Starting with a predefined distribution

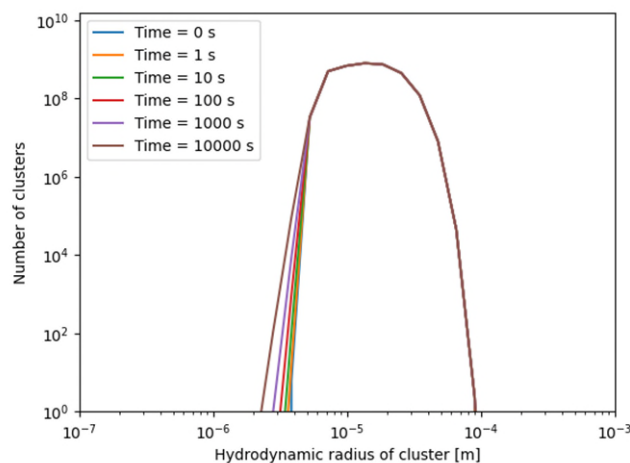


Figure 19: Change of cluster size distribution over the course of 3 hours, given a realistic starting concentration.

Several tests were also done to see how the model predicts that a distribution will evolve when it is given a distribution of particles that corresponds to experimental results, rather than only monomeric particles. The starting concentration distribution was taken from earlier work from KWR, [42] with the starting parameters given in Table 2 (particle concentration replaced with the given distribution).

It is immediately apparent that the evolution of cluster size distribution is rather small, with only a small increase at the lower end of the distribution due to breaking of larger clusters. Due to the difference in sizes between the particles, this only corresponds to a negligible decrease on the right side. Our model is thus able to calculate that systems reach a situation resembling eventual steady-state: only a very small development is observed over the course of three hours, meaning that cluster breakage and growth exist in relatively similar amounts. This reflects reality, as cluster growth tends to plateau over time. [48]

7 Conclusions

In this project, we set out to write a softsensor for the coagulation-flocculation process as is performed by water companies. A softsensor was developed that can predict the cluster size as a function of time during the coagulation-flocculation process. The input for this softsensor is readily available and measurable input data, which is intended for use by water companies themselves. The softsensor has been validated using data KWR published in scientific literature. It corresponds with the experimental findings to a certain point, but improvements can be made on this front. The current version of the softsensor can predict floc cluster size quite well, which is a necessary step for the translation into contaminant removal efficiency. This is intended to be developed in later iterations of this model. The necessary foundation for further iterations have thus been laid for further development towards practical use by water companies.

The softsensor described in this report is a cost-effective method to predict the conditions and outcomes of a coagulation-flocculation process, using only parameters that are readily accessible for water companies as input. Obtaining the same information that the model provides experimentally is an expensive and time-consuming process, and using our softsensor uses only a fraction of the time and cost. Finally, this model is both a broad and essential step towards a comprehensive and generic coagulation-flocculation softsensor: it lays the necessary groundwork for the incorporation of effects of DOC or phosphate capture, cluster removal efficiency using sedimentation, flotation or filtration, or cluster growth under different pH conditions.

8 Future recommendations

We believe several steps would be useful for adding functionality to the softsensor. We depict this in a flowchart of the model, seen in Figure 21.

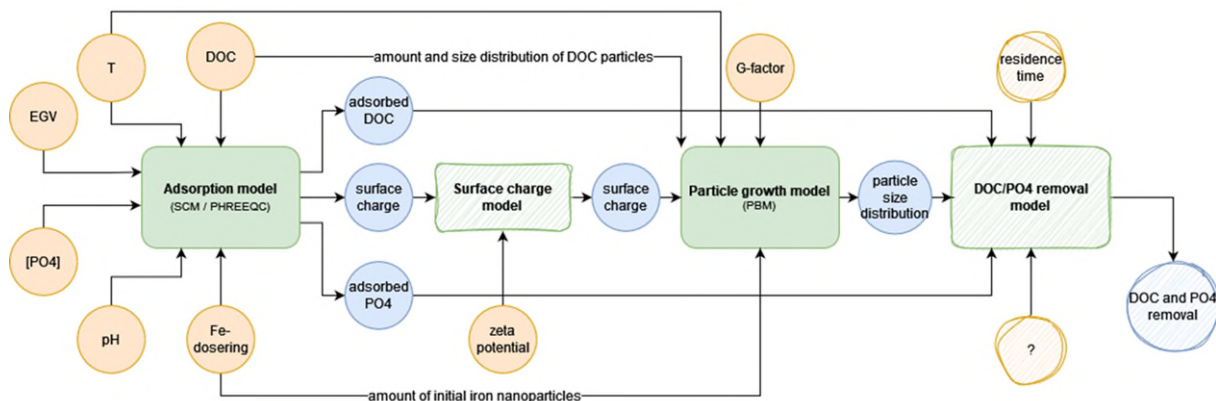


Figure 20: Flowchart of the softsensor. Orange circles are input parameters, blue circles are output parameters, and rectangles are model modules. Unclear lines indicate that this model has not yet been implemented.

We view two steps to be the most promising gaps in our study that can be incorporated into the future model: an oppositely-charged compound model module, for instance by adding DOC/PO₄, and a surface charge model module.

Incorporating DOC in the model, and thus considering oppositely charged moieties in the system leads to complex but likely solvable problems. In this work we used the experimental finding that the particles are slightly negatively charged, but this is expected to have an effect when for instance pH is changed. However, since DOC is generally negatively charged and ferrihydrite tends to be positive, electrostatic effects are no longer purely repulsive. This affects several parts of the model, as the probability of two clusters aggregating now becomes more complex. Furthermore, due to for instance the long-range attractions, fractal dimensions in these systems rise to 2.7. [47] This need to be accommodated for as well. This last point also leads to the fact that cluster structures vary according to the charge balance in a cluster, which is largely determined by the DOC-to-ferrihydrite ratio. This means that a one-dimensional Population Balance model table might not be sufficient, with a two-dimensional table possibly being necessary. In practical terms, this would mean that the softsensor would be able to predict DOC removal efficiency, which is one of the end goals of the softsensor. The development of this functionality would mean that the softsensor can be used for interpreting all coagulation-flocculation processes using ferric chloride as flocculant. This includes the different subprocesses often described in treatment technology such as adsorptive or sweep coagulation.

As for the surface charge model, it would encompass the question of how to *accurately* translate a measured zeta potential to a local surface charge density. As clusters often have irregular surfaces with uneven charge distributions, and the zeta potential being a measurement of the charge potential *averaged over the cluster surface*, translating one into the other is certainly possible given our structural knowledge, but not straightforward. As it is currently unknown how using the zeta potential instead of the surface charge density affects the final results, it might cause unpredictable results down the line. Understanding the link between zeta potentials for these clusters can therefore prevent possible problems in the future and help us develop a better-quality model.

We believe that these two steps would allow our softsensor to have useful predictive strength regarding flocculation behavior in DOC or phosphate-containing systems.

9 References

- [1] S. A. Parsons and B. Jefferson, *Introduction to Potable Water Treatment Processes*, London: Blackwell Publishing Ltd, 2006.
- [2] J. Duan and J. Gregory, "Coagulation by hydrolysing metal salts," *Advances in Colloid and Interface Science*, Vols. 100-102, pp. 475-502, 2003.
- [3] C. Y. Teh, P. M. Budiman, K. P. Y. Shak and T. Y. Wu, "Recent Advancement of Coagulation–Flocculation and Its Application in Wastewater Treatment," *Industrial & Engineering Chemistry Research*, vol. 55, no. 16, pp. 4363-4389, 2016.
- [4] J.-Q. Jiang, "The role of coagulation in water treatment," *Current Opinion in Chemical Engineering*, vol. 8, pp. 36-44, 2015.
- [5] T. Hiemstra, "Formation, stability, and solubility of metal oxide nanoparticles: Surface entropy, enthalpy, and free energy of ferrihydrite," *Geochimica et Cosmochimica Acta*, vol. 158, pp. 179-198, 2015.
- [6] L. Benjamin, *Water quality engineering: physical/chemical treatment processes*, New York: Wiley, 2013.
- [7] N. Thanh, S. Maclean and S. Mahiddine, "Mechanisms of Nucleation and Growth of Nanoparticles in Solution," *Chemical Reviews*, pp. 7610-7630, 2014.
- [8] J. Polte, "Fundamental growth principles of colloidal metal nanoparticles – a new perspective," *CrystEngComm*, pp. 6809-6830, 2015.
- [9] C. W. Neil, J. R. Ray, B. Lee and Y.-S. Jun, "Fractal aggregation and disaggregation of newly formed iron(III) (hydr)oxide nanoparticles in the presence of natural organic matter and arsenic," *Environmental Science: Nano*, vol. 3, pp. 647-656, 2016.
- [10] J. Lee, J. Yang, S. G. Kwon and T. Hyeon, "Nonclassical nucleation and growth of inorganic nanoparticles," *Nature Reviews Materials*, vol. 1, p. 16034, 2016.
- [11] J. Liu, S. M. Louie, C. Pham, C. Da, D. Liang and Y. Hu, "Aggregation of ferrihydrite nanoparticles: Effects of pH, electrolytes, and organics," *Environmental Research*, vol. 172, pp. 552-560, 2019.
- [12] B. Derjaguin and L. Landau, "Theory of the stability of strongly charged lyophobic sols and of the adhesion of strongly charged particles in solutions of electrolytes," *Acta Physico Chimica URSS*, vol. 14, p. 633, 1941.
- [13] E. Verwey and J. Overbeek, "Theory of the stability of lyophobic colloids," *The Journal of Physical and Colloid Chemistry*, vol. 51, no. 3, pp. 631-636, 1948.
- [14] S. H. a. B. M. a. S. P. Behrens, "Aggregation in Charge-Stabilized Colloidal Suspensions Revisited," *Langmuir*, vol. 14, no. 8, pp. 1951-1954, 1998.
- [15] P. Sandkühler, J. Sefcik and M. Morbidelli, "Kinetics of Aggregation and Gel Formation in Concentrated Polystyrene Colloids," *Journal of Physical Chemistry B*, vol. 108, no. 52, pp. 20105-20121, 2004.
- [16] L. Derrendinger and G. Sposito, "Flocculation Kinetics and Cluster Morphology in Illite/NaCl Suspensions," *Journal of Colloid and Interface Science*, vol. 222, pp. 1-11, 2000.
- [17] J. Immink, *Fluids, Gels and Crystals: Phase behavior of binary thermoresponsive microgel mixtures*, Lund: Media-Tryck Sverige, 2019.

- [18] L. Gmachowski, "Aggregate restructuring and its effect on the aggregate size distribution," *Colloids and Surfaces A: Physicochemical and Engineering Aspects*, vol. 207, no. 1-3, pp. 271-277, 2002.
- [19] M. Lattuada, H. Wu and M. Morbidelli, "Hydrodynamic radius of fractal clusters," *Journal of Colloid and Interface Science*, vol. 268, no. 1, pp. 96-105, 2003.
- [20] W. van Saarloos, "On the hydrodynamic radius of fractal aggregates," *Physica A: Statistical Mechanics and its Applications*, vol. 147, no. 1-2, pp. 280-296, 1987.
- [21] S. Tanga, J. M. Preece, C. M. McFarlane and Z. Zhang, "Fractal Morphology and Breakage of DLCA and RLCA Aggregates," *Journal of Colloid and Interface Science*, vol. 221, no. 1, pp. 114-123, 2000.
- [22] S. Romer, F. Scheffold and P. Schurtenberger, "Sol-Gel Transition of Concentrated Colloidal Suspensions," *Physical Review Letters*, vol. 85, p. 4980, 2000.
- [23] M. Lattuada, H. Wu and M. Morbidelli, "Hydrodynamic radius of fractal clusters," *Journal of Physical and Colloid Science*, vol. 268, no. 1, pp. 96-105, 2003.
- [24] S. Lazzari, L. Nicoud, B. Jaquet, M. Lattuada and M. Morbidelli, "Fractal-like structures in colloid science," *Advances in Colloid and Interface Science*, vol. 235, pp. 1-13, 2016.
- [25] D. Ramkrishna and M. Singh, "Population Balance Modeling: Current Status and Future Prospects," *Annual Review of Chemical and Biomolecular Engineering*, vol. 5, pp. 123-146, 2014.
- [26] R. I. Jeldres, P. D. Fawell and B. J. Florio, "Population balance modelling to describe the particle aggregation process: A review," *Powder Technology*, vol. 326, pp. 190-207, 2018.
- [27] J. Liu, Y. Gao, D. Cao, L. Zhang and Z. Guo, "Nanoparticle Dispersion and Aggregation in Polymer Nanocomposites: Insights from Molecular Dynamics Simulation," *Langmuir*, vol. 27, no. 12, pp. 7926-7933, 2011.
- [28] S. J. Smith, K. Page, H. Kim, B. J. Campbell, J. Boerio-Goates and B. F. Woodfield, "Novel Synthesis and Structural Analysis of Ferrihydrite," *Inorganic Chemistry*, vol. 51, no. 11, pp. 6421-6424, 2012.
- [29] M. Zhu, C. Frandsen, A. F. Wallace, B. Legg, S. Khalid, H. Zhang, S. Mørup, J. F. Banfield and G. A. Waychunas, "Precipitation pathways for ferrihydrite formation in acidic solutions," *Geochimica et Cosmochimica Acta*, vol. 172, pp. 247-264, 2016.
- [30] A. Zaccone, H. Wu, D. Gentili and M. Morbidelli, "Theory of activated-rate processes under shear with application to shear-induced aggregation of colloids," *Physical Review E*, p. 051404, 2009.
- [31] O. Guven, "Application of DLVO Theory on the Interaction Forces," *Modern Concepts in Material Science*, vol. 2, no. 5, 2020.
- [32] J. Liu, C. Dai and Y. Hu, "Aqueous aggregation behavior of citric acid coated magnetite nanoparticles," *Environmental Research*, vol. 161, pp. 49-60, 2018.
- [33] B. Faure, G. Salazar-Alvarez and L. Bergström, "Hamaker Constants of Iron Oxide Nanoparticles," *Langmuir*, vol. 27, pp. 8659-8664, 2011.
- [34] T. Tosco, J. Bosch, R. U. Meckenstock and R. Sethi, "Transport of Ferrihydrite Nanoparticles in Saturated Porous Media: Role of Ionic Strength and Flow Rate," *Environ. Sci. Technol.*, vol. 46, no. 7, pp. 4008-4015, 2012.
- [35] R. Angelico, A. Ceglie, H. Ji-Zheng, L. Yu-Rong, G. Palumbo and C. Colombo, "Particle size, charge and colloidal stability of humic acids coprecipitated with Ferrihydrite," *Chemosphere*, vol. 99, pp. 239-247, 2014.
- [36] P. Liao, W. Li, D. Wang, Y. Jiang, C. Pan, J. D. Fortner and S. Yuan, "Effect of reduced humic acid on the transport of ferrihydrite nanoparticles under anoxic conditions," *Water Research*, vol. 109, pp. 347-357, 2017.
- [37] C. Shen, B. Li, Y. Huang and Y. Jin, "Kinetics of Coupled Primary- and Secondary-Minimum Deposition of Colloids under Unfavorable Chemical Conditions," *Environmental Science Technology*, vol. 41, no. 20, pp. 6976-6982, 2007.

- [38] A. Thill, S. Moustier, J. Aziz, M. R. Wiesner and J. Y. Bottero, "Flocs Restructuring during Aggregation: Experimental Evidence and Numerical Simulation," *Journal of Colloid and Interface Science*, vol. 243, no. 1, pp. 171-182, 2001.
- [39] P. Vainshtein, M. Shapiro and C. Gutfinger, "Mobility of permeable aggregates: effects of shape and porosity," *Journal of Aerosol Science*, vol. 35, no. 3, pp. 383-404, 2004.
- [40] Y. Harshe and M. Lattuada, "Universal Breakup of Colloidal Clusters in Simple Shear Flow," *Journal of Physical Chemistry B*, vol. 120, no. 29, pp. 7244-7252, 2016.
- [41] J. D. Pandya and L. A. Spielman, "Floc breakage in agitated suspensions: Effect of agitation rate," *Chemical Engineering Science*, vol. 38, no. 12, pp. 1983-1992, 1983.
- [42] A. S. Ahmad, L. de Waal, P. Volvaard, C. van Genuchten, H. Bruning, E. Cornelissen and A. van der Wal, "Impact of phosphate, silicate and natural organic matter on the size of Fe(III) precipitates and arsenate co-precipitation efficiency in calcium containing water," *Separation and Purification Technology*, vol. 241, p. 116644, 2020.
- [43] S. Jungblut, J.-O. Joswig and A. Eychmüller, "Diffusion- and reaction-limited cluster aggregation revisited," *Phys. Chem. Chem. Phys.*, vol. 21, pp. 5723-5729, 2019.
- [44] Z. Li, S. Shakiba, N. Deng, J. Chen, S. M. Louie and Y. Hu, "Natural Organic Matter (NOM) Imparts Molecular-Weight-Dependent Steric Stabilization or Electrostatic Destabilization to Ferrihydrite Nanoparticles," *Environmental Science and Technology*, vol. 54, no. 11, pp. 6761-6770, 2020.
- [45] L. M. Anovitz, X. Zhang, J. Soltis, E. Nakouzi, A. J. Krzysko, J. Chun, G. K. Schenter, T. R. Graham, K. M. Rosso, J. J. De Yoreo, A. G. Stack, M. Bleuel, C. Gagnon, D. F. R. Mildner, J. Ilavsky and I. Kuzmenko, "Effects of Ionic Strength, Salt, and pH on Aggregation of Boehmite Nanocrystals: Tumbler Small-Angle Neutron and X-ray Scattering and Imaging Analysis," *Langmuir*, vol. 34, no. 51, pp. 15839-15853, 2018.
- [46] A. Beauvois, D. Vantelon, J. Jestin, C. Rivard, M. Bouhnik-Le Coz, A. Dupont, V. Briois, T. Bizien, A. Sorrentino, B. Wu, M. -S. Appavou, E. Lotfi-Kalahroodi, A.-C. Pierson-Wickmann and M. Davranche, "How does calcium drive the structural organization of iron-organic matter aggregates? A multiscale investigation," *Environmental Science: Nano*, vol. 7, pp. 2833-2849, 2020.
- [47] B. Lo and T. D. Waite, "Structure of Hydrous Ferric Oxide Aggregates," *Journal of Colloid and Interface Science*, vol. 222, no. 1, pp. 83-89, 2000.
- [48] W. Yu, C. Hu, H. Liu and J. Qu, "Effect of dosage strategy on Al-humic flocs growth and re-growth," *Colloids and Surfaces A: Physicochemical and Engineering Aspects*, vol. 404, pp. 106-111, 2012.
- [49] B. Yu and B. Li, "Fractal-like tree networks reducing the thermal conductivity," *Physical Review E*, vol. 73, p. 066302, 2006.

I Brinkman's model

$$\Omega_i = \frac{2\xi^2 \left(1 - \frac{\tanh\xi}{\xi}\right)}{2\xi^2 + 3 \left(1 - \frac{\tanh\xi}{\xi}\right)}$$

$$\eta_i = 1 - \frac{d}{\xi} - \frac{c}{\xi^3}$$

$$\xi = \frac{d_a}{\sqrt{K}}$$

$$d = \frac{3}{J} \xi^3 \left(1 - \frac{\tanh\xi}{\xi}\right)$$

$$c = -\frac{1}{J} \left(\xi^5 + 6\xi^3 - \frac{\tanh\xi}{\xi} (3\xi^5 + 6\xi^3) \right)$$

$$J = 2\xi^2 + 3 - 3 \frac{\tanh\xi}{\xi}$$

$$K = \frac{d_p^2}{72} \left(3 + \frac{3}{1-\phi} - \sqrt[3]{\frac{8}{1-\phi}} - 3 \right)$$

$$\phi = 1 - C \left(\frac{d_a}{d_p} \right)^{d_f-3}$$

$$u_i = \frac{(\rho_p - \rho_l)gR_i^2}{9\mu}$$

• Ω_i	Drag force correction	[-]
• η_i	Fluid accumulation efficiency	[-]
• d_p	Monomeric (primary) particle diameter	[m]
• d_a	Aggregate particle diameter	[m]
• C	Packing coefficient, assumed to be 1	[-]
• ϕ	Porosity	[-]
• d_f	Fractal dimension	[-]
• ρ_i	Particle density	[kg m ⁻³]
• g	Gravitational constant	[N m ² kg ⁻²]
• μ	Viscosity	[kg m ⁻¹ s ⁻¹]

This model contains a lot of parameters, each of which can be determined mathematically. By assuming a packing coefficient of 1, an assumption that is generally done in the scientific literature, we only need the primary particle diameter, the aggregate diameter and the fractal dimension to calculate the drag force corrections and fluid accumulation efficiencies. Other parameters are unnamed because they are simple intermediate unitless variables that do not have any physical meaning.

